A Three-Phase Delta Switch Rectifier for More Electric Aircraft Applications Employing a Novel PWM Current Control Concept

M. Hartmann, J. Miniboeck and J. W. Kolar
Power Electronic Systems Laboratory
Swiss Federal Institute of Technology
Zurich, Switzerland
Email: hartmann@lem.ee.ethz.ch

***Abstract*— In the course of the More Electric Aircraft program active three-phase rectifiers in the power range of 5 kW are required. A comparison with other rectifier topologies shows that the three-phase Δ-switch rectifier (comprising three Δ-connected bidirectional switches) is well suited for this application. The system is analyzed using space vector calculus and a novel PWM current controller concept is presented, where all three phases are controlled simultaneously; the analysis shows that the proposed concept yields optimized switching sequences. To facilitate the rectifier design, analytical relationships for calculating the power components average and rms current ratings are derived. Furthermore, a laboratory prototype with an output power of 5 kW is realized. Measurements taken from this prototype confirm the operation of the proposed current controller. Finally, initial EMI-measurements of the system are also presented.**

I. Introduction

In modern aircraft the trend is to replace hydraulically driven actuators for flight control surfaces, such as rudder and aileron, by Electro Hydrostatic Actuators (EHA) in order to implement the "More Electric Aircraft" concept (MEA) [1]-[3]. The EHA units are connected to the aircraft power system by three-phase rectifiers with typical specifications as listed in TABLE I. The MEA-concept in general calls for a reduction in the size and weight of the electrical systems. A major issue is the weight reduction of the power generation system by eliminating the generator gearbox, which however will result in a variable mains frequency of 360 Hz... 800 Hz. Additional, the electronic systems must have very high reliability, i.e. the loss of one phase must not result in an outage of the rectifier system. Furthermore, the loads are not allowed to feed back energy into the mains and therefore unidirectional rectifiers have to be used. Due to the very rigorous current harmonic limits of present airborne system standards, PWM-rectifiers with low THD of the input current and for a high total power factor are required.

In [4] it has been shown that the 6-switch three-level Vienna-type rectifier topology (cf. **Fig. 1(a)**) [5] is very well suited for aircraft applications. This topology's main feature is a reduced semiconductor voltage stress, especially of importance for high output voltage levels. However, the trade-off is increased conduction losses since there are always two semiconductors connected in series per phase. Two-level three-phase rectifier topologies may show better efficiencies but suffer from higher semiconductor voltage stress.

TABLE I: Typical specifications of active three-phase rectifiers in aircraft applications.

$V_{N,i}$	115 V $\pm$ 15%
f_{in}	360 Hz ... 800 Hz
V_o	400 V_{DC}
P_o	5 kW ... 10 kW

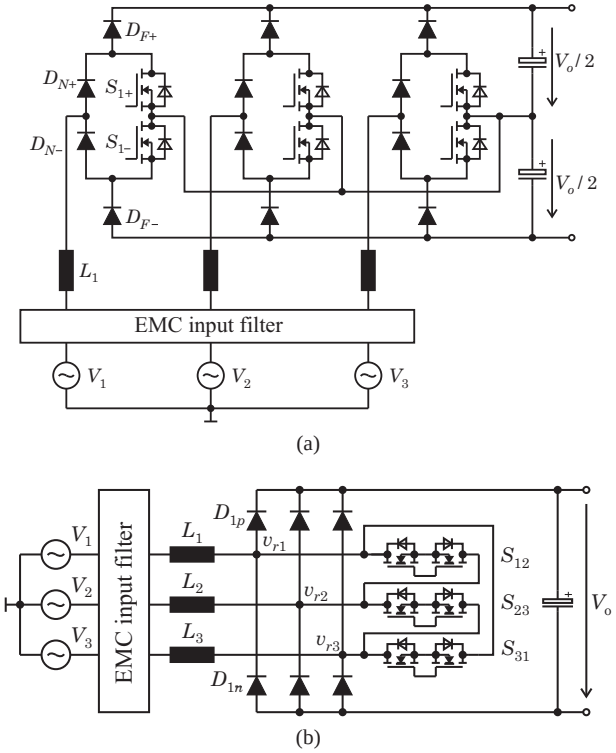

Fig. 1: Active three-phase rectifiers suitable for aircraft applications; (a) three-level 6-switch Vienna-type rectifier and (b) two-level Δ-switch rectifier.

For the desired output voltage level of $V_o = 400\,V_{DC}$, high efficiency switches (CoolMOS) with a blocking voltage of 600 V and $R_{DSon} < 100\,m\Omega$ are commercially available. Hence, a reduction of the voltage stress, as given by three-level topologies like the Vienna-Rectifier concept, is not needed. Several two-level three-phase rectifier topologies are presented in the literature and a comparative study can be found in [6]-[7]. The application of a standard six-switch PWM-rectifier bridge is not favourable because of its bidirectional power flow behavior. Additional drawbacks are the reduced reliability because of possible shoot-through of a bridge leg, resulting in a short circuit of the DC-voltage, the high current levels of the semiconductors and the involvement of the MOSFET body diode, causing a substantial limitation of the switching frequency. In [9] a topology using either Y-connected or Δ-connected (cf. **Fig. 1(b)**) bidirectional switches on the AC-side

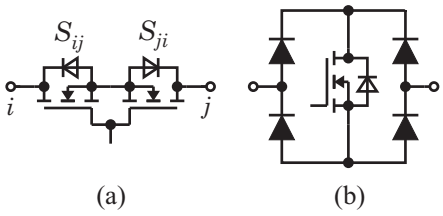

Fig. 2: Possible realizations of a bidirectional (current), bipolar (voltage) switch using (a) two MOSFETs and (b) a MOSFET and a diode bridge.

is presented. In general, the Y-connected realization shows higher conduction losses as compared to the Δ-connected alternative, since there are always two (bidirectional) switches connected in series. A short-circuit of the DC-voltage is not possible with both topologies. **Fig. 2** shows two possibilities of realizing the bidirectional (current), bipolar (voltage) switches. The original Vienna-Rectifier topology uses the bidirectional switch shown in **Fig. 2(b)** instead of the two MOSFETs per phase-leg shown in **Fig. 1(a)**. An elegant topology, which integrates the bidirectional switch of **Fig. 2(b)** into the diode bridge, is presented in [10]-[11]. However, the conduction losses of this realization are higher than for the realization using two MOSFETs (**Fig. 1(a)**). Also, some topologies using quasi tri-directional switches [12] or topologies operating in discontinuous conduction mode were presented [13]-[14]. The topology using tri-directional switches increases the system complexity and discontinuous-mode topologies cannot fulfil the requirements on the total harmonic distortion. Due to its low complexity, low conduction losses and high reliability the Δ-switch rectifier topology seems to be an optimal choice for realization of a rectifier for aerospace applications with the requirements in TABLE I.

Besides efficiency and power density, control issues also influence the practical applicability of the circuit topology. Several possibilities for the control of three-phase rectifiers exist and a survey of these methods can be found in [15]. A control method based on low switching frequencies is given in [16] but cannot be used for the desired application because of the high AC current harmonics. A hysteresis controller as shown in [17] would be an easy way to control the rectifier system, but its varying switching frequency may increase the effort of EMI-filtering. A controller using the one-cycle control method is presented in [18], but there the controller structure has to be changed over every $60°$ and the input current control is always limited to 2 phases. In [19]-[20] a PWM-control method for the rectifier system is proposed, however, no information was given about the exact switching sequence of the switches, which mainly influences the efficiency of the rectifier system.
In this work a novel PWM-control method using triangular carrier signals is presented where all three phases are controlled simultaneously. The resulting optimal switching sequences are analyzed by application of space vector calculus. Additionally, the proposed control method is able to handle a phase loss without changing the controller structure.

II. System Operation

The three switches S_{ij} $(i,j \in \{1,2,3\})$ of **Fig. 1(b)** are used to generate sinusoidal input currents which are proportional to the mains voltage. The discrete converter voltage space vector can be

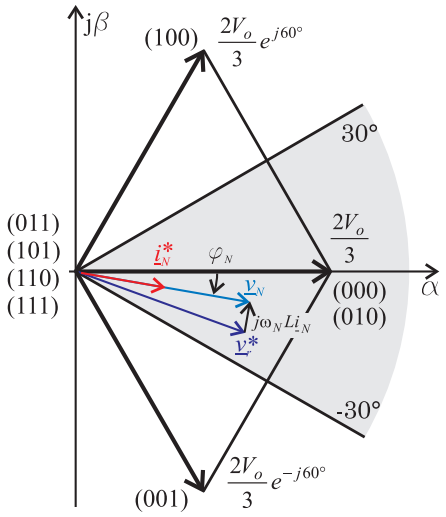

Fig. 3: Space vector diagram of the Δ-switch rectifier for the sector $\varphi_N \in [-30°, +30°]$.

calculated by

$$\underline{v}_r = \frac{2}{3}(v_{r1} + \underline{a}v_{r2} + \underline{a}^2 v_{r3}) \text{ with } \underline{a} = e^{j\frac{2\pi}{3}} \ . \tag{1}$$

The possible converter voltages v_{ri} are dependent on the state of the switches s_{ij} ($s_{ij} = 1$ denotes the turn-on state of switch S_{ij}) and on the direction of the input phase currents i_{Ni}. Therefore, the available voltage space vectors change over every $60°$ of the mains frequency. If (s_{12}, s_{23}, s_{31}) describes the different switching states, the resulting voltage space vectors for $\varphi_N \in [-30°, 30°]$ ($i_{N1} > 0$, $i_{N2} < 0$, $i_{N3} < 0$) can be calculated as

$$(000), (010) : \underline{v}_{r_1} = \frac{2}{3}V_o \tag{2}$$

$$(001) : \underline{v}_{r_2} = \frac{2}{3}V_o e^{-j60°} \tag{3}$$

$$(100) : \underline{v}_{r_3} = \frac{2}{3}V_o e^{j60°} \tag{4}$$

$$(011), (101), (110), (111) : \underline{v}_{r_4} = 0 \tag{5}$$

(cf. **Fig. 3**).

Only states (000), (001), (010) and (100) show a non-zero magnitude and the voltage space vector of (010) is equal to the space vector for state (000). In each $60°$-sector there is a redundancy of the (000)-vector and therefore only 4 different voltage space vectors can be generated by the converter in each sector. These discrete voltage space vectors are used to approximate the converter's voltage reference vector

$$\underline{v}_r^* = \widehat{\underline{V}}_r^* \ e^{j\varphi_{v_r}} \ , \ \varphi_{v_r} = \omega_N t \tag{6}$$

in the time average over the pulse-period. In conjunction with the mains voltage system

$$\underline{v}_N = \widehat{\underline{V}}_N \ e^{j\varphi_{\underline{v}_N}} \tag{7}$$

the voltage difference

$$\underline{v}_N - \underline{v}_r^* = L\frac{d\underline{i}_N^*}{dt} \tag{8}$$

leads to the input current

$$\underline{i}_N^* = \widehat{\underline{I}}_N^* \ e^{j\varphi_{\underline{i}_N}} \ , \tag{9}$$

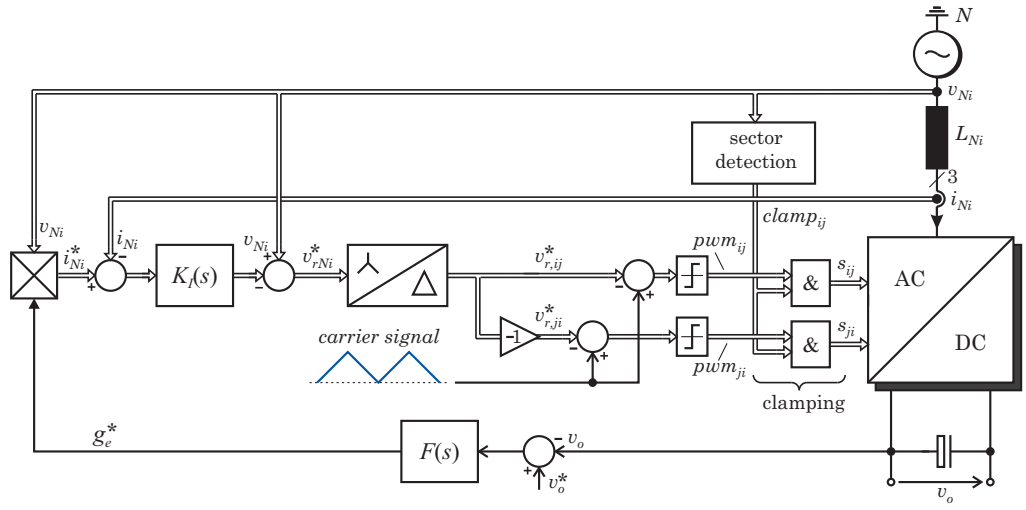

Fig. 4: Structure of the proposed PWM-current controller. Signal paths being equal for different phases are shown by double lines.

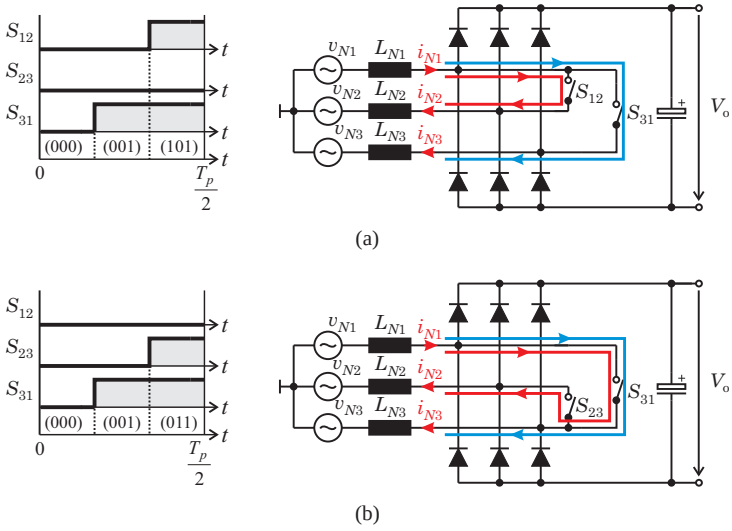

Fig. 5: Possible switching sequences for $\varphi_N = -15°$ and equivalent circuits for the time interval where both switches are on; (a) Sequence A: (000)-(001)-(101)-(001)-(000), $S_{23} = \text{OFF}$; (b) Sequence B: (000)-(001)-(011)-(001)-(000), $S_{12} = \text{OFF}$.

if only average values over one pulse period are considered. All voltage space vectors with two or three switches in the on-state, are redundant and hence only two switches can be used to control the input currents. The remaining switch has to be permanently off in this sector. Two different switching sequences can be generated in each 60°-sector. **Fig. 5** shows the corresponding modulation signals of the bidirectional switches ($\varphi_N = -15°$), and equivalent circuits are given for the time interval where both switches are on. For sequence A ((000)-(001)-(101)-(001)-(000), $S_{23} = \text{OFF}$), the positive input current i_{N1} is shared by S_{12} and S_{31} dependent on the on-states of the switches. In contrast to sequence A, the whole current i_{N1} is carried by switch S_{31} for sequence B ((000)-(001)-(011)-(001)-(000), $S_{12} = \text{OFF}$) during the state (011). This results in higher conduction losses and therefore sequence A is preferable.

III. Novel PWM Current Controller

The aim of the current controller is to force the input currents of each phase to follow the (sinusoidal) mains voltages. However, the Δ-connected switches directly influence the line-to-line voltages. Therefore, the idea is near at hand of controlling these Δ-related currents. Unfortunately, this is not very convenient because of the necessary clamping actions caused by the large number of redundant switching states. This can be avoided if the phase currents i_{Ni} of the rectifier are controlled. The resulting phase modulation signals then have to be transferred to Δ-oriented quantities. In this way all three currents can be controlled permanently and the necessary clamping actions are performed in a final logic unit just before the PWM-signals s_{ij} are transferred to the switches.

The structure of the proposed current controller is shown in **Fig. 4**. All three input currents i_{Ni} are sensed by an appropriate current sensor and compared with the reference current i^*_{Ni}. The reference current is generated by multiplying the mains voltage v_{Ni} by a reference conductance g^*_e (defined by the superimposed output voltage controller $F(s)$) in order to achieve ohmic input current behavior. Together with a mains voltage feed-forward signal [21], the current controller $K_I(s)$ (realized as P-type controller) generates the required converter phase voltages v^*_{rNi}. The bidirectional switches are connected between two phases and therefore the corresponding equivalent line-to-line converter voltages

$$v^*_{r12} = v^*_{rN1} - v^*_{rN2} \tag{10}$$
$$v^*_{r23} = v^*_{rN2} - v^*_{rN3} \tag{11}$$
$$v^*_{r31} = v^*_{rN3} - v^*_{rN1} \tag{12}$$

are needed for PWM-generation. The delta-star transformation is followed by two PWM-modulators which generate the PWM-signals for the MOSFETs of the bidirectional switches (bidirectional switches are realized according to **Fig. 2(a)**). In general, dependent on the current direction of the bidirectional switch, only one MOSFET has to be gated. If the second MOSFET is permanently off during this time, the current is carried by its body diode. Unfortunately, this body diode shows a relative large forward voltage which yields to higher conduction losses. These losses can be reduced by the low-impedance path of the MOSFET channel, if the second MOSFET is turned on as well. Since the current direction of the switch only changes every 120°, this MOSFET can be permanently on during this time interval. Hence, two independent PWM-signals are required for the bidirectional switches. As shown in **Fig. 2(a)**, MOSFET S_{ij} connects port i of the bidirectional switch to port j and its PWM-signals are given

by pwm_{ij} respectively. The operation of the modulator will be discussed in the next section.

The clamping actions are controlled by a sector-detection unit which derives the clamping signals $clamp_{ij}$ from the mains voltage. The resulting clamping actions considering all $60°$-sectors are summarized in TABLE II for all MOSFETs, whereas i.e. 0 indicates that the corresponding MOSFET is permanently off in this sector.

A. PWM modulator

For realization of the PWM-modulator a single unipolar triangle carrier signal is used (cf. **Fig. 6**). The modulator has to assure an optimal switching sequence and has to generate the duty cycles

$$v^*_{rij} > 0: \quad \delta_{ij} = 1 - \frac{v^*_{rij}}{V_o}\,, \qquad \delta_{ji} = 1 \tag{13}$$

$$v^*_{rij} < 0: \quad \delta_{ij} = 1\,, \qquad \delta_{ji} = 1 - \frac{v^*_{rji}}{V_o}\,. \tag{14}$$

If the carrier signal is larger than the modulation voltage v^*_{rij}, the output of the modulator is high. Unlike the triangle signal, the modulation voltages v^*_{rij} are bipolar and hence a duty cycle of 100% is generated for negative modulation voltages. According to

$$v^*_{rij} = (-1) \cdot v^*_{rji}\,, \tag{15}$$

one MOSFET of the bidirectional switch is always permanently on (i.e. S_{21} for $\varphi_N \in [-30°, 30°]$), which reduces the on-state losses of the device.

Fig. 6 shows the operation of the PWM-modulator at $\varphi_N = -15°$. The two modulation voltages v^*_{r21} and v^*_{r31} are negative and result in a duty cycle of 100%. According to TABLE II, switches S_{23} and S_{32} are permanently off in this sector and are therefore not shown. The remaining voltages v^*_{r12} and v^*_{13} are used for modulation and result in the desired optimal switching sequence (000)-(001)-(101)-(001)-(000) (see also **Fig. 5**).

IV. Simulation Results

A simulation is used to confirm the operation of the proposed control technique. **Fig. 7(a)** demonstrates a good performance of the proposed current controller at an input frequency of $f_{in} = 800\,\mathrm{Hz}$ ($V_{Ni} = 115\,\mathrm{V_{rms}}$, $V_o = 400\,\mathrm{V_{DC}}$, $P_o = 5\,\mathrm{kW}$, $L_{Ni} = 330\,\mu\mathrm{H}$). The input currents I_{Ni} follow the sinusoidal 800 Hz input voltages V_{Ni}, even for a rather limited switching frequency of 72 kHz. Furthermore, the current ripple of the clamped phase is not higher than in the two controlled phases. It has to be mentioned again that the current controller works permanently (i.e without any structural changes) and that only a logic-block just before the modulator output provides the necessary clamping actions. In **Fig. 7(b)** the system response on a phase loss at

TABLE II: Required clamping actions; 0 indicates that the corresponding MOSFET is permanently off; 1 permanently on and pwm_{ij} that the MOSFET is modulated by the current controller.

	s_{12}	s_{21}	s_{23}	s_{32}	s_{13}	s_{31}
$330° \ldots 30°$	pwm_{12}	1	0	0	pwm_{13}	1
$30° \ldots 90°$	0	0	pwm_{23}	1	pwm_{13}	1
$90° \ldots 150°$	1	pwm_{21}	pwm_{23}	1	0	0
$150° \ldots 210°$	1	pwm_{21}	0	0	1	pwm_{31}
$210° \ldots 270°$	0	0	1	pwm_{32}	1	pwm_{31}
$270° \ldots 330°$	pwm_{12}	1	1	pwm_{32}	0	0

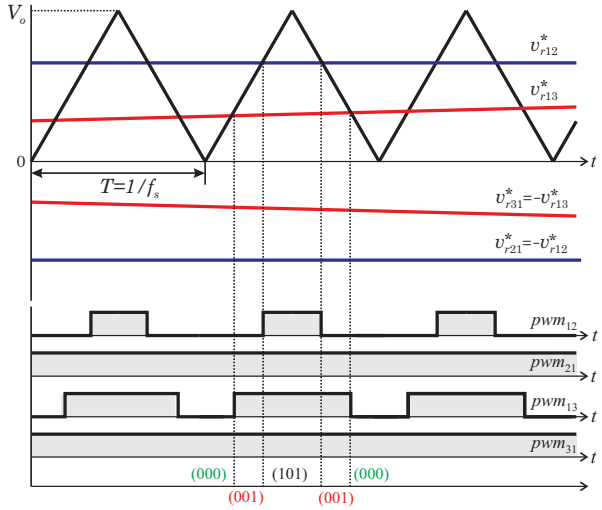

Fig. 6: PWM-modulation and resulting switching sequence at $\varphi_N = -15°$. Switches S_{23} and S_{32} are not shown, because they are permanently off in this sector. The resulting (optimal) sequence is (000)-(001)-(101)-(001)-(000).

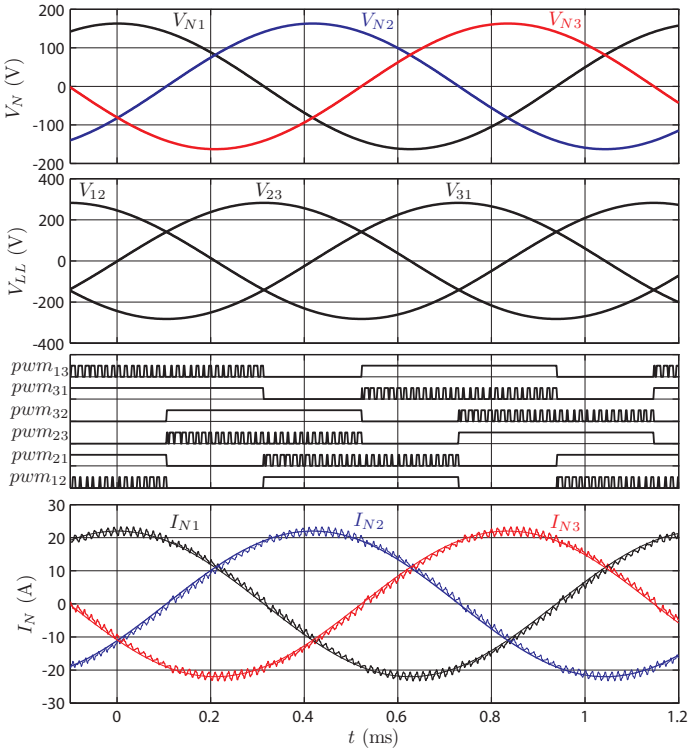

(a)

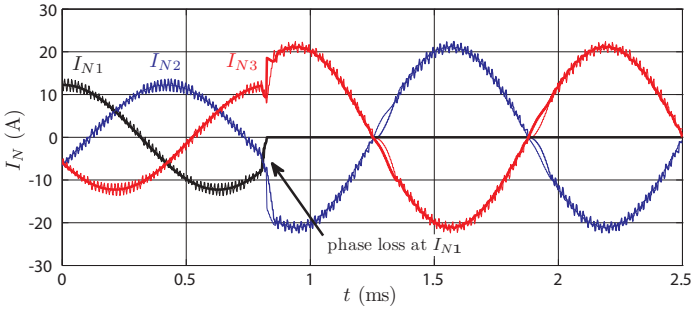

(b)

Fig. 7: Simulation results of the Δ-switch rectifier; (a) $V_{Ni} = 115\,\mathrm{V_{rms}}$, $f_{in} = 800\,\mathrm{Hz}$, $V_o = 400\,\mathrm{V_{DC}}$, $P_o = 5\,\mathrm{kW}$, $L_{Ni} = 330\,\mu\mathrm{H}$ and (b) phase loss of I_{N1} at $t = 0.85\,\mathrm{ms}$ ($P_o = 3\,\mathrm{kW}$).

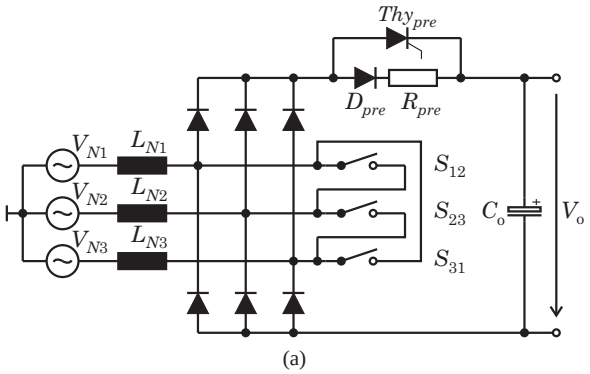

(a)

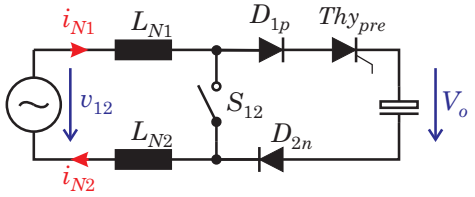

(b)

Fig. 8: (a) Proposed precharge circuit for startup of the rectifier, consisting of precharge diode D_{pre}, precharge resistor R_{pre} and thyristor Thy_{pre} and (b) equivalent circuit for switch S_{12} at $\varphi_N = -15°$.

$t = 0.85\,\mathrm{ms}$ is depicted. After some minor ringing, the system operates in 2-phase mode and it should be noticed that no changes in the controller structure or parameters are required to handle this fault condition.

V. System Design

In this section some issues of the design and the practical realization of the Δ-switch rectifier shall be discussed.

A. Startup

A precharge circuit consisting of diode D_{pre}, resistor R_{pre} and thyristor Thy_{pre} is applied on the DC-side of the rectifier (cf. **Fig. 8(a)**) in order to limit the inrush current at the rectifier startup. During startup, the thyristor is off and the precharge resistor limits the inrush current. The thyristor is turned on as soon as the capacitors are completely charged to the peak value of the line-to-line voltage. The bidirectional switches are permanently off during startup (current controller is disabled during this time). According to **Fig. 8(b)**, the thyristor is located within the commutation path of the rectifier (i.e. $S_{12}, D_{1p}, Thy_{pre}$ and D_{n2}). In order to minimize the thyristors influence on the parasitic inductance of the commutation path, three thyristors (one thyristor closely placed to each switch) are used in parallel. This also reduces the on-resistance of the additional element advantageously.

B. Component Stresses

In order to determine the on-state losses of the semiconductors, the current rms and average values have to be calculated and therefore simple analytical approximations are derived. For the following calculations it is assumed that the rectifier has

- a purely sinusoidal phase current shape;
- ohmic fundamental mains behavior;
- no low-frequency voltage drop across the boost inductor for the sinusoidal shaping of the input currents;
- a constant switching frequency;
- linear behavior of the boost inductors (inductance is not dependent on the current level).

TABLE III: Analytically calculated and simulated mean and rms current values of the semiconductors for $P_o = 4\,\mathrm{kW}$, $V_{Ni} = 115\,\mathrm{V_{rms}}$ ($M = 0.7$), $f_s = 72\,\mathrm{kHz}$, $L_{Ni} = 330\,\mu\mathrm{H}$

	Simulated	**Calculated**
$\widehat{I}_N$	16.5 A	16.5 A
$I_{T,avg}$	0.98 A	0.95 A
$I_{T,rms}$	3.09 A	3.0 A
$I_{D,avg}$	3.33 A	3.35 A
$I_{D,rms}$	6.53 A	6.56 A
$I_{Thy,avg}$	10.0 A	10.06 A
$I_{Thy,rms}$	12.3 A	12.35 A
$I_{C,rms}$	7.16 A	7.16 A

1) Bidirectional switches S_{ij}

Each bidirectional switch of **Fig. 2(a)** consists of two MOSFETs and hence two elements have to be considered: the MOSFET which is modulated by the current controller and the body-diode of the second MOSFET. Therefore, the current average values of the semiconductors are not zero, although the entire average current of the bidirectional switch is zero (averaging within a full line-frequency fundamental period). With the defined modulation index

$$M = \frac{\sqrt{3}\widehat{V}_N}{V_o}\,, \tag{16}$$

the average and rms currents of the two semiconductors forming the bidirectional switch finally result in:

$$I_{T,avg} = \widehat{I}_N \left(\frac{1}{2\pi} - \frac{M}{4\sqrt{3}}\right)\,, \tag{17}$$

$$I_{T,rms} = \widehat{I}_N \sqrt{\left(\frac{1}{6} - \frac{\sqrt{3}}{8\pi}\right) - \frac{M}{2\sqrt{3}\pi}}\,. \tag{18}$$

2) Diodes D_{pi}, D_{ni}

The average and rms-currents of the rectifier diodes are

$$I_{D,avg} = \widehat{I}_N \frac{M}{2\sqrt{3}}\,, \tag{19}$$

$$I_{D,rms} = \widehat{I}_N \sqrt{\frac{M\left(5 + 2\sqrt{3}\right)}{12\pi}}\,. \tag{20}$$

3) Startup Thyristor Thy_i

The thyristor current is a combination of the diode currents, and results to

$$I_{Thy,avg} = 3 \cdot I_{D,avg} = \widehat{I}_N \frac{M\sqrt{3}}{2}\,, \tag{21}$$

$$I_{Thy,rms} = \widehat{I}_N \sqrt{\frac{5M}{2\pi}}\,. \tag{22}$$

4) Capacitor C_o

The rms current stress of the output capacitor for a constant load current I_o can be calculated using

$$I_{C,rms} = \sqrt{I_{Thy,rms}^2 - I_{Thy,avg}^2}\,, \tag{23}$$

which leads to

$$I_{C,rms} = \widehat{I}_N \sqrt{\frac{5M}{2\pi} - \frac{3M^2}{4}}\,. \tag{24}$$

To verify the derived formulas the mean and rms currents for an output power of 4 kW and mains voltage of $V_{Ni} = 115\,\mathrm{V_{rms}}$ ($M = 0.7$) have been calculated. In TABLE III the results of this calculation are compared to the results of a simulation and show a good accuracy.

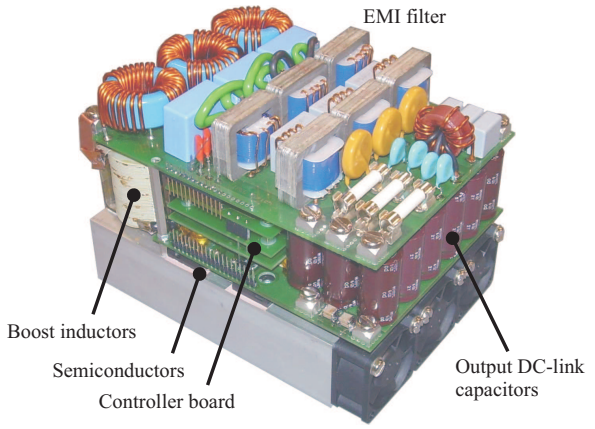

Fig. 9: 5 kW Δ-switch rectifier laboratory prototype. Dimensions: 66.9 in x 47.2 in x 49.2 in

TABLE IV: Specifications of the realized prototype.

Input voltage:	$v_{in} = 97\,\mathrm{V_{rms}} \ldots 115\,\mathrm{V_{rms}}$
Input frequency:	$f_{in} = 360\,\mathrm{Hz} \ldots 800\,\mathrm{Hz}$
Switching frequency:	$f_s = 72\,\mathrm{kHz}$
Output voltage:	$v_{out} = 400\,\mathrm{V_{DC}}$
Output power:	$P_{out} = 5\,\mathrm{kW}$

TABLE V: Power devices selected for realization of the Δ-switch rectifier.

Part	**Device Description**
S_{ij}	IPW60R045CP (CoolMOS)
D_{ni}, D_{pi}	APT30D60BHB (Ultrafast)
Thy_i	40TPS12A
C_{out}	18 x Nippon Chemicon KXG 82 µF/450 V in parallel
L_{Ni}	Schott HWT-193, 326 µH

VI. Laboratory Prototype

Based on the proposed controller concept a laboratory setup of the Δ-switch rectifier according to the specifications given in TABLE IV has been built. The realized prototype is shown in **Fig. 9**. An existing EMI-filter, originally designed for a 72 kHz Vienna-type rectifier, also was applied to this rectifier. The overall dimensions of the system are 66.9 in x 47.2 in x 49.2 in, thus giving a power density of $2.35\,\mathrm{kW/dm^3}$ (or $38.5\,\mathrm{W/in^3}$). The system is air cooled and has a weight of 3.78 kg which results in a power to weight ratio of 1.32 kW/kg. The proposed controller is digitally implemented in a fixed point Texas Instruments DSP (TI 320F2808) and a switching frequency of 72 kHz is used. For realization of the bidirectional switches, the CoolMOS IPP60R045CP with a very low R_{DSon} of $45\,\mathrm{m\Omega}$ is used and the rectifier diodes are realized by APT30D60BHB. A summary of the employed devices is given in TABLE V.

A. Calculated and Measured Efficiency

The losses and efficiency of the realized rectifier are calculated for $f_{in} = 400\,\mathrm{Hz}$ using the analytical expressions derived in section V based on the datasheet specifications (components listed in TABLE V). The results of this calculation are given in TABLE VI.

The losses of the Δ-switch rectifier are dominated by the losses of the semiconductors. For the desired input voltage range the calculated efficiency varies between 94% and 95.2% and the results are in good agreement with the measurement results given in **Fig. 10**. The measured efficiencies are somewhat lower than the calculated values and the difference has been found in the current dependent losses of the EMI-filter. For the sake of brevity these losses have been considered as a constant term in the calculation. A three-phase power source [22] is used for testing the rectifer and the limited output current capability of the power source (5 kW, $13\,\mathrm{A_{rms}}$) limits the power level for the efficiency measurements.

TABLE VI: Calculated power loss break-down and efficiency of the proposed Δ-switch rectifier for an output power of $P_o = 4\,\mathrm{kW}$.

Input voltage (line rms)	97.7	115	132	V
Input voltage (line-to-line rms)	169	199	229	V
Input current (rms)	14.4	12.2	10.6	A
Modulation index	0.6	0.7	0.81	
Losses				
Switch losses	67.4	54.3	45.3	W
Diode losses	23.9	23.2	22.6	W
Thyristor losses	10.8	10.6	10.3	W
Total semiconductor losses	102.1	88.1	78.2	W
Input choke	34	30	27	W
Output capacitors	12	8	5	W
Auxiliary power	30	30	30	W
Additional losses (EMI,...)	70	70	70	W
Total power losses	249.1	226.1	210.2	W
Efficiency	94.0	94.6	95.1	%

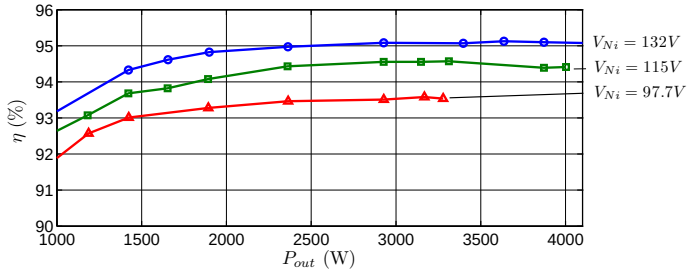

Fig. 10: Measured efficiency of the 5 kW laboratory prototype at $f_{in} = 400\,\mathrm{Hz}$ for the specified mains voltages.

B. Experimental results

The input currents of the rectifier are given in **Fig. 12(a)** for an output power of 4 kW, where a $\mathrm{THD_I}$ of 3.2 % and a power factor of $\lambda = 0.999$ have been measured. In **Fig. 12(b)** the inductor current I_{N1} is shown. The current ripple is in good agreement with the simulation results and confirms the operation of the proposed current controller. As mentioned in section V, the commutation paths include four semiconductor devices. Therefore, it is difficult to minimize the parasitic inductance of this path in a practical realization. The result is a considerable ringing of the MOSFETs drain-source voltages. In **Fig. 13**, a measurement of the drain-source voltage v_{DS} of switch S_{12} is shown. Although the layout has been optimized to minimize the commutation path inductance, a voltage overshoot of $\approx 60\,\mathrm{V}$ can be observed in case the switch is PWM-operated. Furthermore (as depicted in **Fig. 13**), the MOSFET additionally experiences a PWM-shaped blocking voltage, originating from the two other switches while the device is clamped into permanently-off state (S_{12} in $\varphi_N \in [30° \ldots 90°, 210° \ldots 270°]$). Unfortunately, this voltage overshoot is even higher than the over-voltage generated from the switch itself which has to be considered in the system design.

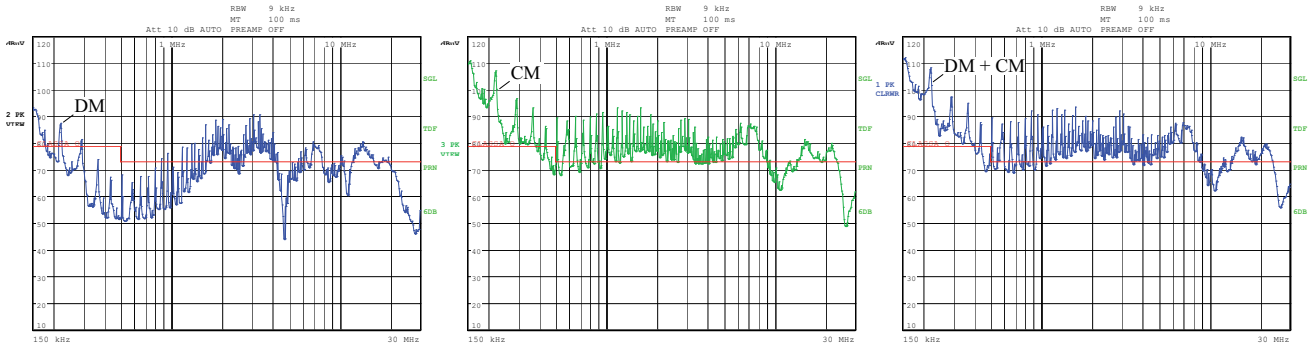

(a) (b) (c)

Fig. 11: First CE measurements; (a) DM emissions, (b) CM emissions and (c) total conducted emissions without EMI-Filter.

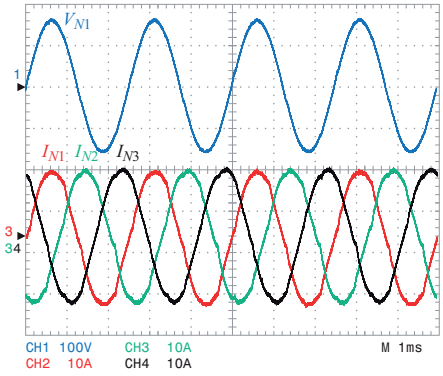

(a)

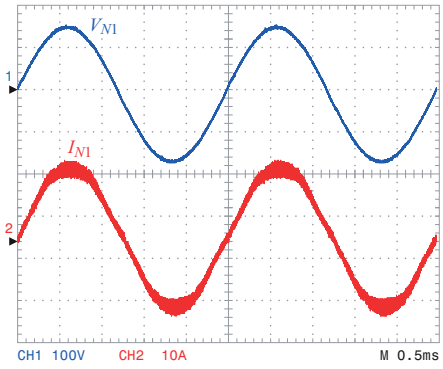

(b)

Fig. 12: Measurement results taken from the laboratory prototype at an output power level of $P_o = 4\,\mathrm{kW}$ and an input frequency of $f_{in} = 400\,\mathrm{Hz}$; (a) all three input currents and (b) inductor current of phase I_{L1}.

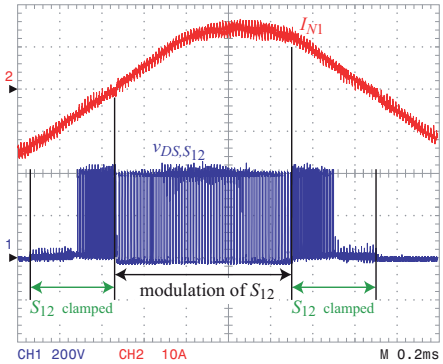

Fig. 13: Measured drain-source voltage v_{DS} of switch S_{12} at an output power level of $P_o = 4\,\mathrm{kW}$.

TABLE VII: Comparison of the proposed Δ-switch rectifier with a 6-switch Vienna-type rectifier.

	Δ-switch rectifier	**6-switch Vienna-type rectifier**
Num. of switches	6	6
Num. of diodes	6	9
Num. of thyristors	3	3
Output voltage	400 V	400 V
Output power	5 kW	5 kW
Efficiency (@115V/5kW)	94.9%	94.4%
Power density	$2.35\,\mathrm{kW/dm^3}$	$2.35\,\mathrm{kW/dm^3}$
Power weight ratio	1.32 kW/kg	1.32 kW/kg

In order to get a basic idea of the conducted emissions of the Δ-switch rectifier, initial EMI-measurements of the rectifier were performed at an input frequency of $f_{in} = 50\,\mathrm{Hz}$. For that purpose a standard LISN according to CISPR 16 ($50\,\mu\mathrm{H}$, $50\,\Omega$) [23] was used. A three-phase DM/CM noise separator [24] was applied to measure the DM and CM noise separately. The measurements were done without a specific EMI-filter, but to provide proper operation of the rectifier capacitors of $3.4\,\mu\mathrm{F}$ per phase have been placed at the input of the rectifier in star connection. The results of the peak-measurement according to CISPR 11 (frequency range $150\,\mathrm{kHz} \ldots 30\,\mathrm{MHz}$) are shown in **Fig. 11** together with the limits of CISPR 11 class A. According to **Fig. 11**, CM emissions dominate the emissions of the converter.

VII. Comparison with Vienna Rectifier

In order to be able to benchmark the characteristics of the proposed Δ-switch rectifier a 6-switch Vienna-type rectifier (cf. **Fig. 1(a)**) is used as reference. Both rectifiers are designed to obtain the specifications listed in TABLE IV. The same semiconductors and power components as listed in TABLE V and also a nearly identical mechanical construction is used for the VR realization. According to TABLE VII, three more diodes are required for the VR, but these diodes are only commutated with the supplying mains frequency and are therefore relatively inexpensive. The D_{N-} diodes of the Vienna-type rectifier are replaced by the startup thyristors, hence no additional elements are needed for startup. The Δ-switch rectifier shows a slightly better efficiency compared to the Vienna-type rectifier system at equal size and power density. If the output voltage of the Vienna-type rectifier is increased to $V_o = 800\,\mathrm{V}$, the Vienna-type rectifier is able to handle input-voltages up to $V_{l,l} = 440\,\mathrm{V_{rms}}$ and an

output power of $P_o = 10\,\mathrm{kW}$ which increases its power density considerably. However, for the desired output voltage range of $V_o = 400\,\mathrm{V_{DC}}$, the Δ-switch rectifier is the optimal choice.

VIII. Conclusion

This paper presents the design of a 5 kW three phase Δ-switch rectifier focused to the application in More Electric Aircraft systems. A comparison to several alternative circuit topologies showed that the Δ-switch rectifier is a very interesting choice for the desired application. For the proposed rectifier a novel optimized PWM-control concept has been designed and analyzed using space vector calculus. Digital simulations demonstrate an excellent performance, even in the case that a phase loss occurs. Analytical expressions for the component stresses are derived that simplify the design and dimensioning of the system. With the realized prototype, a $\mathrm{THD_I}$ of 3.2% at $f_{in} = 400\,\mathrm{Hz}$ and an efficiency of 94.6% at $P_o = 4\,\mathrm{kW}$ have been achieved, which results in a power density of $2.35\,\mathrm{kW/dm^3}$ and a power to weight ratio of 1.32 kW/kg. Measurements taken from the realized 5 kW laboratory prototype confirm the high performance of this novel current controller. Finally, first EMI-measurements of the converter are presented. A comparison of the Δ-switch rectifier with a 6-switch Vienna-type rectifier certifies a slightly higher efficiency for the Δ-switch rectifier.

References

[1] D.R. Trainer, C.R. Whitley, "Electric actuation - power quality management of aerospace flight control systems," *Proc. of the Internat. Conference on Power Electronics, Machines and Drives 2002*, 4-7 June 2002, pp. 229-234.

[2] J.A. Rosero, J.A. Ortega, E. Aldabas, L.Romeral, "Moving towards a more electric aircraft," *IEEE Magazine on Aerospace and Electronic Systems*, Vol.22, No.3, March 2007, pp.3-9.

[3] C.R. Avery, S.G. Burrow, P.H. Mellor, "Electrical generation and distribution for the more electric aircraft," *Proc. of the 42nd International Universities Power Engineering Conference (UPEC 2007)*, 4-6 Sept. 2007, pp.1007-1012.

[4] G. Gong et al., "Comparative evaluation of three-phase high-power-factor AC-DC converter concepts for application in future More Electric Aircraft," *IEEE Transactions on Industrial Electronics*, Vol.52, No.3, June 2005, pp. 727-737l.

[5] Yifan Zhao, Yue Li, T.A. Lipo, "Force commutated three level boost type rectifier," *IEEE Transactions on Industry Applications*, Vol.31, No.1, Jan/Feb 1995, pp.155-161.

[6] J.C. Salmon, "Comparative evaluation of circuit topologies for 1-phase and 3-phase boost rectifiers operated with a low current distortion," *Proc. of Canadian Conference on Electrical and Computer Engineering, Halifax, NS, Canada (1994)*, 25-28 Sep. 1994, Vol.1, pp. 30-33.

[7] J.C. Salmon, "Reliable 3-phase PWM boost rectifiers employing a series-connected dual boost converter sub-topology," *Conf. Rec. of IEEE Industry Applications Society Annual Meeting (1994),*, 2-6 Oct 1994 vol.2, pp. 781-788.

[8] J.C. Salmon, "3-phase PWM boost rectifier circuit topologies using 2-level and 3-level asymmetrical half-bridges," *Proc of the 10th Annual Applied Power Electronics Conference and Exposition (APEC'95)*, 5-9 Mar 1995, Vol.2, pp.842-848.

[9] J.W. Kolar, H. Ertl, F.C. Zach, "Realization considerations for unidirectional three-phase PWM rectifier systems with low effects on the mains," *Proc. of the 6th Int. Conf. on Power Electronics and Motion (PEMC 1990)*, Budapest.

[10] P. Bialoskorski, W. Koczara, "Unity power factor three phase rectifiers," *Proc. of the 24th Annual IEEE Power Electronics Specialists Conference (PESC '93)*, 20-24 Jun 1993, pp.669-674.

[11] W. Koczara, P. Bialoskorski, "Controllability of the simple three phase rectifier operating with unity power factor," *Proc of the 5th European Conference on Power Electronics and Applications*, 13-16 Sep 1993, Vol.7, pp.183-187.

[12] D. Carlton, W.G. Dunford, M. Edmunds, "Continuous conduction mode operation of a three-phase power factor correction circuit with quasi tri-directional switches," *Proc. of the 30th Annual IEEE Power Electronics Specialists Conference (PESC 99)*, Aug 1999, vol.1, pp.205-210.

[13] D. Carlton, W.G. Dunford, M. Edmunds, "'Deltafly' three-phase boost power factor correction circuit operating in discontinuous conduction mode," *Proc. of the IEEE International Symposium on Industrial Electronics (ISIE '99)*, 1999, vol.2, pp.533-538.

[14] D. Carlton, W.G. Dunford, M. Edmunds, "SEPIC 3-phase 3-switches power factor correction circuit operating in discontinuous conduction mode," *Proc. of the IEEE International Symposium on Industrial Electronics (ISIE '98)*, 7-10 Jul 1998, Vol.1, pp.81-86.

[15] M.P. Kazmierkowski, L. Malesani, "Current control techniques for three-phase voltage-source PWM converters: a survey," *IEEE Transactions on Industrial Electronics*, Vol.45, No.5, Oct 1998, pp.691-703.

[16] A. Lima, C. Cruz, F. Antunes, "A new low cost AC-DC converter with high input power factor," *Proc. of the 22nd IEEE International Conference on Industrial Electronics, Control, and Instrumentation (IECON'96)*, 5-10 Aug 1996, Vol.3, pp.1808-1813.

[17] R.J. Tu; C.L. Chen, "A new space-vector-modulated control for a unidirectional three-phase switch-mode rectifier," *IEEE Transactions on Industrial Electronics*, Vol.45, No.2, Apr 1998, pp.256-262.

[18] C. Qiao; K.M. Smedley, "A general three-phase PFC controller for rectifiers with a parallel-connected dual boost topology," *IEEE Transactions on Power Electronics*, Vol.17, No.6, Nov 2002, pp. 925-934.

[19] N. Noor, J. Ewanchuk, J.C. Salmon, "PWM current controllers for a family of 3-switch utility rectifier topologies," *Proc. of the Canadian Conference on Electrical and Computer Engineering (CCECE 2007)*, 22-26 April 2007, pp.1141-1144.

[20] J.C. Salmon, J.C., "Reliable 3-phase PWM boost rectifiers employing a stacked dual boost converter subtopology," *IEEE Transactions on Industry Applications*, Vol.32, No.3, May/Jun 1996, pp.542-551.

[21] M. Chen; J. Sun, "Feedforward current control of boost single-phase PFC converters," *Proc. of the 19th Annual IEEE Applied Power Electronics Conference and Exposition (APEC '04)*, Vol.2, 2004, pp. 1187-1193.

[22] Elgar Electronics Corp., "SmartWave switching amplifier SW5250A, Operation Manual," http://www.elgar.com (2008).

[23] IEC Internationl Special Committee on Ratio Interference - C.I.S.P.R.(1977), "C.I.S.P.R. Specification for Radio Interference Measuring Apparatur and Measurement Methods - Publication 16," Geneve, Switzerland.

[24] M.L. Heldwein et al., "Novel three-phase CM/DM conducted emissions separator," *Proc. of the 20th Annual IEEE Applied Power Electronics Conference and Exposition (APEC 2005)*, 6-10 March 2005 Vol.2, pp.797-802.